

First-principles study of the effect of Fe impurities in MgO at geophysically relevant pressures

Donat J. Adams*

Dep. Materials Sciences, Lab. Crystallography, ETH Zürich, Switzerland[†]

W.M. Temmerman and Z. Szotek

Daresbury Laboratory, Daresbury, Warrington WA4 4AD, United Kingdom

(Dated: February 3, 2022)

The self-interaction corrected local spin density (SIC-LSD) formalism and the standard GGA treatment of the exchange-correlation energy have been applied to study the collapse of the magnetic moment of Fe impurities in MgO. The system $\text{Mg}_{1-x}\text{Fe}_x\text{O}$ is believed to be the second most abundant mineral in the Earth's lower mantle. We confirm the experimentally found increase of the critical pressure upon iron concentration. Our calculations using standard GGA for a fixed Fe concentration show that different arrangements of Fe atoms can remarkably shift the transition pressure of the high spin (HS) to low spin (LS) transition. This could explain the experimentally found broad transition regions. Our results indicate that the HS-LS transition in $\text{Mg}_{1-x}\text{Fe}_x\text{O}$ is first order. We find that SIC-LSD fails to predict the divalent Fe configuration as the lowest energy configuration and discuss possible reasons for it.

PACS numbers: 71.27.+a, 71.15.Mb

I. INTRODUCTION

The high spin (HS) to low spin (LS) transitions in magnesiowüstite, $\text{Mg}_{1-x}\text{Fe}_x\text{O}$, and wüstite, Fe_{1-x}O , are of great geophysical importance. Magnesiowüstite is believed to be the second most abundant mineral in the Earth's mantle.^{1,2} While MgO was thoroughly studied both in theory and experiment^{3,4,5,6,7,8,9,10,11,12,13,14,15,16} at high pressures, few theoretical studies exist for $\text{Mg}_{1-x}\text{Fe}_x\text{O}$ mainly because of the difficulty to treat the effects of strong correlation for the Fe-3d orbitals.^{17,18,19} The magnetic phase transition could strongly influence the partition coefficient of Fe between MgO and MgSiO_3 perovskite and postperovskite,²⁰ dramatically change radiative conductivities,²¹ and lead to a hardening of the materials.²² However, magnesiowüstite $\text{Mg}_{1-x}\text{Fe}_x\text{O}$ and wüstite Fe_{1-x}O have been studied in numerous experimental papers.^{20,23,24,25,26,27,28} The main problem has been, that wüstite exists only as a non-stoichiometric compound.^{19,29,30,31,32} There is a general consensus that its rocksalt-type structure contains a fully occupied O^{2-} sublattice, while Fe exists predominantly in the form of Fe^{2+} , with some Fe^{3+} , as well as vacancies and interstitials, exhibiting a short range order. The resulting clusters arrange with a long range order, which – depending on the density of interstitials – can be commensurate or incommensurate.^{25,26,27,28}

For Fe_{1-x}O Jacobsen et al.³³ reported a transition from a cubic to a rhombohedral phase at a pressure between 22.8 GPa and 27.7 GPa at room temperature. At low temperatures, on the other hand, Struzhkin et al.³⁴ found a phase transition from a cubic to a rhombohedral structure with a Néel-temperature of $T_N = 198$ K at ambient pressure. At ambient temperature this transition is shifted to a pressure of 15 GPa.

At pressures of 85 to 143 GPa a magnetic high-spin to low-spin transition was observed in several experiments.^{19,32,35} Some studies find a broad transition region,³⁵ while in others³² the transition is first order. Differential stress might have smeared out the phase transition over a broad region in some studies or small compositional differences within the sample

could have changed the transition behavior.

Recent developments in high pressure physics allowed to investigate the LS-HS transition in magnesiowüstite. Badro et al.²⁰ and Lin et al.²⁴ could prove what was suggested a long time before:² the complete electronic rearrangement of Fe in $\text{Mg}_{1-x}\text{Fe}_x\text{O}$ under pressure, while the NaCl-type structure remains stable across the phase transition. The transition pressures are in reasonable agreement (49 to 75 GPa for $x = 0.15$,²⁰ 50 to 60 GPa for $x = 0.25$ ²⁴). The transition is linked to a hardening of the materials and a decrease of the molar volume (across the phase transition: $V_{\text{OLS}}/V_{\text{OHS}} = 0.904$, bulk modulus: $K_{\text{OT}}^{\text{HS}} = 160.7$ GPa, $K_{\text{OT}}^{\text{LS}} = 250$ GPa²⁴).

In another study the HS-LS transition in $\text{Mg}_{1-x}\text{Fe}_x\text{O}$ was studied for different iron concentrations ($x = 0.2, 0.5$ and 0.8).³⁶ The transition pressure turns out to depend linearly on the Fe concentration and is 40, 60 and 80 GPa, respectively. For $\text{Fe}_{0.97}\text{O}$ the transition pressure is shifted to 90 GPa. At high Fe concentration ($x = 17\%$) Badro et al.³⁷ in an X-ray emission study find that the HS state is stable up to 143 GPa, whereas Pasternak et al.³⁵ conjecture from Mössbauer spectroscopy a strong temperature dependence of the transition pressure. They found the transition to be completed only at 120 GPa ($\text{Fe}_{0.94}\text{O}$) at 450 K.

In the present paper we study the effect of Fe impurities in MgO at geophysically relevant pressures, using self-interaction corrected local spin density (SIC-LSD) method which allows to treat the localized *d* electrons of Fe on equal footing with the other itinerant electrons. In addition, we use GGA approach and the VASP code³⁸ to study the influence of possible Fe impurity clustering in the MgO supercells on the relevant transition pressures. The aim is to realize different Fe concentrations in MgO and investigate their effect on the experimentally observed properties.

The outline of the paper is as follows. In Section II, we briefly describe the SIC-LSD methodology. Section III concentrates on the discussion of the present SIC-LSD and GGA results, while Section IV concludes the paper.

II. METHODOLOGY

A. The self-interaction corrected LSD

The standard LSD approximation for the exchange-correlation energy introduces an unphysical interaction of an electron with itself, the so-called self-interaction (SI). It is the aim of the self-interaction corrected local spin density approximation to construct a self-interaction free energy functional

$$E_{\text{SIC}} = E_{\text{LSD}} - \sum_{\alpha} \delta_{\alpha}^{\text{SIC}}, \quad (1)$$

where α numbers the occupied orbitals and the self-interaction correction (SIC), $\delta_{\alpha}^{\text{SIC}}$, of the orbital α is

$$\delta_{\alpha}^{\text{SIC}} = U[n_{\alpha}] + E_{\text{xc}}^{\text{LSD}}[\bar{n}_{\alpha}]. \quad (2)$$

It is known that the exact exchange-correlation energy $E_{\text{xc}}[\bar{n}_{\alpha}]$, depending on the spin density \bar{n}_{α} , for the case of a single electron orbital with electron density n_{α} , cancels the Hartree energy $U[n_{\alpha}]$ identically:

$$U[n_{\alpha}] + E_{\text{xc}}[\bar{n}_{\alpha}] = 0. \quad (3)$$

In the case of approximate exchange-correlation energy functionals this cancellation can be guaranteed by Eq. 1.

Varying the above SIC-LSD energy functional with respect to the orbital spin densities, with the constraint that the ϕ_{α} 's form a set of orthonormal functions, one gets the SIC-LSD generalized eigenvalue equations

$$H_{\alpha} | \phi_{\alpha} \rangle = \left(H_{0\sigma} + V_{\alpha}^{\text{SIC}}(\mathbf{r}) \right) | \phi_{\alpha} \rangle = \sum_{\alpha'} \lambda_{\alpha\alpha'} | \phi_{\alpha'} \rangle, \quad (4)$$

with $H_{0\sigma}$ being the orbital independent LSD Hamiltonian. The Lagrangian multipliers $\lambda_{\alpha\alpha'}$ are used to secure the fulfillment of the orthonormality constraint.

Due to the orbital dependent SIC potential, V_{α}^{SIC} , the SIC energy functional is not stationary with respect to infinitesimal unitary transformations among the orbitals. The so-called localization criterion

$$\langle \phi_{\beta} | V_{\alpha}^{\text{SIC}} - V_{\beta}^{\text{SIC}} | \phi_{\alpha} \rangle = 0 \quad \forall(\alpha, \beta) \quad (5)$$

has to be fulfilled to ensure that the solutions of the SIC-LSD equations (4) are most optimally localized to reach the absolute minimum of the SIC-LSD functional (1).

The SIC-LSD approach is fully *ab initio* and introduces no adjustable parameters, either for the delocalized (band-like) or localized electrons. For extended states the SIC vanishes. The SIC-LSD formalism has the advantage that it allows to compare different valence states and spin configurations of the same atom. The nominal valence, N_{val} , in the SIC-LSD approach is defined as

$$N_{\text{val}} = Z - N_{\text{core}} - N_{\text{SIC}}, \quad (6)$$

TABLE I: The most relevant spin configurations of Fe, labeled HS and LS according to Ref. 36. Here HS state corresponds to the case where SIC is applied to all the majority and one minority electrons. For realizing LS state, SIC is applied to the three majority and three minority t_{2g} electron states. The HS³ stands for the trivalent Fe configuration, where all the majority d electrons are treated as localized, by applying SIC. The calculations with applying no SI-corrections have been labeled lsd. All possible electronic configurations with five or six SI-corrected orbitals namely trivalent and divalent ions have been considered in the present study. However, the ones listed below correspond to the lowest enthalpies. Here 1 means that a given state has been SI-corrected, and 0 otherwise.

	Majority channel					Minority channel				
	t_{2g}	t_{2g}	e_g	t_{2g}	e_g	t_{2g}	t_{2g}	e_g	t_{2g}	e_g
HS	1	1	1	1	1	1	0	0	0	0
LS	1	1	0	1	0	1	1	0	1	0
HS ³	1	1	1	1	1	0	0	0	0	0

where Z is the atomic number, N_{core} is the number of core (and semicore) states and N_{SIC} is the number of self-interaction corrected states. The ground state valence is the one defined by the ground state energy. In our application of SIC-LSD to (Mg,Fe)O all possible electron configurations of the Fe atom with five and six SI-corrected d orbitals have been considered.⁶⁵ The most energetically relevant ones are given in Table I. The energy functional without any SIC states is simply equivalent to the standard LSD approximation and labelled lsd in the following. Thus LSD is a local minimum of the SIC-LSD functional, corresponding to the case when all the electrons are treated as itinerant and described by the Bloch wave functions. The choice of the SIC orbital configuration, i. e. the number and symmetry of localized vs. delocalized states, can significantly influence the corresponding total energy. The electronic configuration giving rise to the most negative total energy, with the most optimally localized orbitals, defines the absolute energy minimum of the SIC-LSD energy functional as well as the corresponding valency.

The SIC-LSD approach used in this work has been implemented in the linear muffin-tin orbitals (LMTO) band structure method with the atomic sphere approximation (ASA).^{39,40,41} The slightly overlapping ASA spheres approximate the polyhedral Wigner-Seitz cell and the sum of their volumes equals to the volume of the actual unit cell. The ASA does not allow for atomic relaxations, as different ionic arrangements will lead to different sphere overlaps. In the LMTO-ASA approach empty spheres (E) can be introduced in order to increase the space filling and to minimize the overlap.

In all the calculations performed with the LMTO-ASA method we have treated the valence states of the Mg-3s, Mg-3p, O-2s, O-2p, Fe-3d, Fe-4s, Fe-4p, E-1s as the so-called low waves, while the Mg-3d, O-3d and E-2p states have been represented as intermediate waves.⁴² All the electrons in lower shells have been put in the core but allowed to relax. The separation of valence electrons into the low and intermediate waves has been done for the purpose of reducing the size of the eigenvalue problem. The secular equation that is fully di-

agonalized is constituted by the low waves and provides the eigenvalues and eigenvectors. The intermediate waves enter the Hamiltonian through their tails, partly retaining their true characteristics.

For both magnesiowüstite and wüstite, we have assumed the ideal rock salt structure. The ASA radii of MgO were adjusted in order to reproduce the experimental band gaps of 7.83 eV.⁴³ Best agreement was found with radii of 1.34646 Å, 1.05313 Å, 0.751847 Å for Mg, O and the interstitial spheres E, with the resulting LDA band gap of 4.7 eV. The total volume of the spheres was equal to the volume of the cell for all the SIC calculations while the ratios of the ASA radii were kept constant. The ASA radius of Fe was equal to the one of Mg.

To realize different concentrations of Fe impurities in the systems studied, three supercells have been used, namely consisting of four, eight and 32 formula units of MgO. By substituting up to four Mg atoms by Fe atoms one could realize Fe concentrations ($x = \frac{n_{\text{Fe}}}{n_{\text{cations}}}$) of 3.125%, 12.5%, 25%, 50% and 100%. For Fe concentrations of 3.125%, 12.5%, 25%, we have chosen the smallest possible supercell of the ideal FCC/NaCl, namely replacing one Mg atom by one Fe atom respectively in the supercells consisting of 32, eight and four formula units. The concentrations of 50% and 100% have been realized using a supercell of eight atoms in total and replacing respectively two and four Mg atoms by Fe atoms. Consequently, both ferromagnetic (FM) and antiferromagnetic (AFM) orders as well as charge disproportionation could be studied. This corresponds to an Fe arrangement with maximal distances between the Fe atoms and would provide the lowest transition pressures. Regarding the AFM structure, the chosen supercells allowed to realize only the so-called AF1 order where the magnetic spins are arranged in parallel in the (001) planes, but are anti-aligned between the planes. The number of k-points has been chosen inversely proportional to the size of the supercell (eight, 16, 64 atoms) and was $16 \times 16 \times 16$, $8 \times 8 \times 8$ and $4 \times 4 \times 4$, respectively. This gives energy differences precise to within 1.7×10^{-6} eV/atom (1.25×10^{-7} Ryd/atom).

B. Pressure determination

The pressures and enthalpies, of relevance to the present study, can be determined from the LMTO-ASA total energy, E , vs. volume, V , calculations through invoking the equation of state (EOS) and fitting to a number of calculated data points.⁶⁶ Specifically, the third-order Birch Murnaghan EOS has been used,^{44,45} namely

$$E(x) = E_0 + \frac{9B_0 V_0}{16} (B'(x^{2/3} - 1)^3 + (x^{2/3} - 1)^2 \times (6 - 4x^{2/3})), \quad (7)$$

$$P(x) = \frac{3B_0}{2} (x^{7/3} - x^{5/3}) \times \left(1 + \frac{3}{4} (B' - 4) \times (x^{2/3} - 1)\right), \quad (8)$$

$$x = \frac{V_0}{V}, \quad (9)$$

allowing to compute the enthalpy H at any volume as $H(V) = E(V) - P(V)V$, with P denoting the pressure. In the above, V_0 stands for the equilibrium volume, B_0 for the bulk modulus and B' for its first pressure derivative.

The calculation of enthalpy differences, $\Delta H(P)$, can be accomplished through the numerical inversion of the pressure in Eq. 8. This allows to compare enthalpies of two spin configurations labelled s and s' at a given pressure:

$$\Delta H^{(s,s')} = H^s(V^s) - H^{s'}(V^{s'}). \quad (10)$$

To determine the theoretical equilibrium volumes and total energies for all the studied scenarios, the lattice parameters have been sampled in the range from -10% up to +16% (relative to the zero-pressure value) in steps of 2%. The resulting volume increase or decrease of -33.1% to 40.7% typically corresponds to a pressure range of -20 GPa to 285 GPa.⁶⁷

III. RESULTS AND DISCUSSION

A. (Mg,Fe)O in the SIC-LSD framework

In the application of SIC-LSD to Fe-doped MgO, we have studied 29 different localization-delocalization scenarios for three different supercells, various Fe concentrations, and symmetries of localized Fe d states. Among all the cases we have identified four energetically relevant configurations, namely the three SIC configurations listed in Table I as well as the LSD solution. This finding has been independent of the actual Fe concentration. The HS configuration is the high-spin divalent scenario, where all majority Fe d states and one minority Fe t_{2g} state are treated as localized through invoking SIC, giving rise to an insulating state. The HS³, trivalent, configuration corresponds to the scenario where only the majority Fe d states are corrected for the self-interaction, and thus localized, constituting a half-metallic state. The LS state corresponds to the case where both majority and minority Fe t_{2g} states are localized by SIC. This naturally leads to a non-magnetic and insulating configuration.

From the enthalpy calculations we find, in disagreement with experimental evidence, that the HS³ and LSD solutions are energetically most favorable, respectively at the low and high pressure regions. This can be seen in Fig. 1(a), where the enthalpy differences, with respect to the HS³ configuration, are plotted as a function of pressure for all the relevant

scenarios and Fe concentration of 3.125%. The trivalent HS^3 state constitutes the ground state solution for all the pressures up to about 140 GPa. However, at very low pressures the divalent HS state lies very close in energy to the HS^3 state and the enthalpy difference, at 0 GPa and 3.125% Fe concentration, is $H_{\text{HS}} - H_{\text{HS}^3} = 0.05$ eV. Note that at this Fe concentration the total energies of the HS and HS^3 configurations, evaluated at their respective theoretical volumes, are fully degenerate.

The nominal valence of the HS^3 state, being 3+, is at odds with the experimental findings, where Fe appears clearly as Fe^{2+} in $(\text{Mg},\text{Fe})\text{O}$ (see e.g. Ref. 20) or with a small ratio of additional Fe^{3+} in Fe_xO (see e.g. Ref. 32). Note, however, that the nominal valence defined in SIC-LSD not always corresponds to the chemical valence. Although the nominal valences of the trivalent and divalent states differ by one (namely 3+ vs. 2+), in terms of a simple charge counting or charge disproportionation, the two ions, corresponding respectively to the HS^3 and HS configurations, differ only by up to 0.1 electron. Similar observation was made by Szotek et al.⁴⁶ for magnetite. Despite the latter, it is still surprising to find the trivalent, instead of the divalent, Fe-state as the lowest energy configuration, in particular for Fe_xO (with $x=1$). This is in variance to the SIC-LSD results obtained for all the other transition metal monoxides, namely MnO , CoO and NiO .^{47,48} It is possible that the failure of SIC-LSD to find the divalent ground state in FeO has its origin in the fact that LSD substantially overestimates the exchange splitting for the systems in question. Consequently, the energy gained on localizing an additional electron to create a divalent Fe ion is not sufficient to overcome that exchange splitting. However, since FeO does not occur in a stoichiometric form, but as Fe_{1-x}O , and experiments indicate existence of both divalent and trivalent ions, one would need to perform more realistic calculations to establish the importance of the off-stoichiometry and valence fluctuations for obtaining the divalent ground state in FeO .

At high pressures, it is the experimentally indicated³⁶ LS configuration that is relevant, with its nominal valence of 2+ in agreement with the experimentally found Fe^{2+} in wüstite and magnesiowüstite. The LS configuration competes with the LSD description of the Fe-3d states, as seen through the corresponding enthalpy difference which at 0 GPa and 3.125% Fe concentration is $H_{\text{lsd}} - H_{\text{LS}} = 0.7$ eV (see Fig. 1), in favour of the LS state, while the LSD becomes energetically more favorable for pressures in the excess of 140 GPa. At such high pressures the gain in band formation energy on delocalization of all the Fe *d* electrons clearly wins with the localization energy of those electrons. Since the magnitude of SIC is strongly dependent on the orbitals, one needs to be guided by energetics in defining the ground state energy and configuration.

Introducing several Fe impurities into a supercell ($\text{Mg}_2\text{Fe}_2\text{O}_4$ and Fe_4O_4) opens a possibility of realizing both parallel (labelled [f], ferromagnetic) and antiparallel (labelled [a], antiferromagnetic \equiv AF1) arrangements of the spin magnetic moments on those Fe atoms. In Fig. 1(b), the enthalpy differences are plotted for the above mentioned configurations, and both parallel and antiparallel arrangements of spins on the Fe atoms in the relevant supercell with 50% Fe concentration. For the HS configuration the [f] and [a]

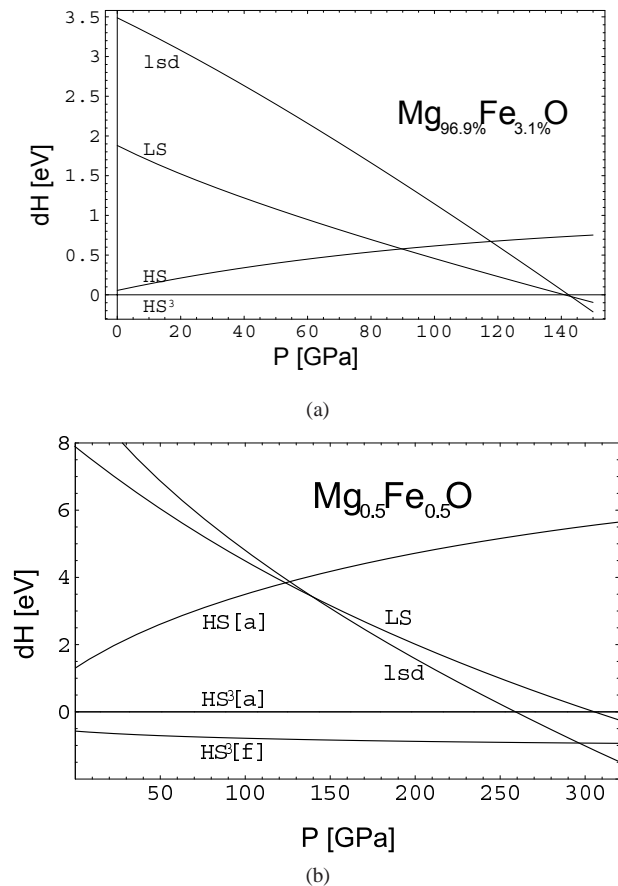


FIG. 1: Enthalpy differences at different Fe concentration x . (a) $x = 3.125\%$. The HS^3 configuration appears to be energetically most favorable up to a pressure of 145 GPa, where a phase transition is predicted to the state where all the Fe-3d delocalize (lsd). The commonly assumed HS configuration is less energetically favourable, and at the pressure of 90 GPa the electrons completely rearrange to the non-polarized configuration LS, although the localization of the electrons is not lost. (b) $x = 50\%$. Two Fe atoms were introduced into a cell containing 8 atoms in total (two Mg, two Fe, four O). Parallel and antiparallel alignments of the spin moments is denoted in brackets [f] and [a], respectively. More than 10 different arrangements with asymmetric charge configurations on the Fe atoms were also tried out, but resulted in high enthalpies. They are omitted in the plot for more clear readability.

arrangements return the same energies while for HS^3 the [f] arrangement appears always lower in energy ($\Delta E = 0.5$ eV for $\text{Mg}_{0.5}\text{Fe}_{0.5}\text{O}$ and $\Delta E = 1.5$ eV FeO ⁶⁸) than the antiparallel alignment.

Finally, we consider the dependence of the HS-LS transition pressure on the concentration of the Fe impurities in a supercell. As can be seen in Fig. 2, our study predicts an increase of this transition pressure with rising Fe concentration. However, the absolute transition pressures for isostructural phase transitions, as calculated in this SIC-LSD study, are higher than the experimental values.⁴⁹ Two possible scenarios can operate at any Fe concentration: a possible transi-

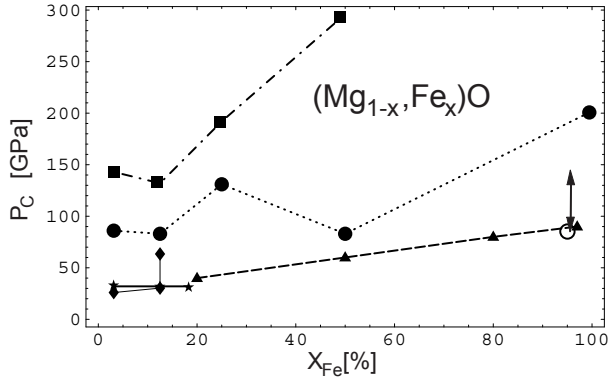


FIG. 2: $\text{Mg}_{1-x}\text{Fe}_x\text{O}$: Experimental and theoretical transition pressures. Squares (■) - SIC-LSD calculations, scenario HS^3 -lsd (electronic configuration HS^3 at low pressures, no SI-corrections at high pressure); bullets (●) - SIC-LSD calculations scenario HS-LS (electronic configuration HS at low pressures, configuration LS at high pressure); lozenges (◆) - GGA-PAW calculations (low concentrations); stars (★) - LDA+U calculations [50]; triangles (▲) - Mössbauer spectroscopy, [36]; arrow (↑) - Mössbauer spectroscopy [35]; circle (○) - X-ray diffraction [32].

tion from HS^3 to lsd or from HS to LS. The second one occurs at considerably lower pressures than the first one, and is the relevant one for comparison with experiments, although leading to a phase diagram in rather poor agreement with experiment. The latter implies the existence of Fe^{2+} , and a low pressure structure with one minority $\text{Fe } t_{2g}$ state and five majority d states.³⁶ One might envisage that the HS state could possibly become favourable if in the SIC-LSD calculations the ionic relaxations had been applied. It is obvious that ASA error can substantially affect total energies, although one would like to hope that these errors would be less severe when considering only the energy differences between different configurations. Also, across the phase transition Fe is known to reduce its ionic radius and therefore the ionic relaxations could significantly reduce the enthalpies of the LS structures which in turn could further decrease the transition pressure.⁶⁹

B. Density of states from SIC-LSD

In Fig. 3, we present the densities of states (DOS) calculated for all the energetically relevant scenarios and the Fe impurity concentration of 12.5%. As can be seen in the figure, at this intermediate concentration the localized Fe-3d states form narrow bands. At higher concentrations of Fe impurities these bands extend over a considerable energy range, e.g. 3-5 eV at 25% of Fe. For the HS and HS^3 configurations, the occupied Fe 3d band states lie below the predominantly O 2p valence band. As mentioned earlier, the SI corrections for the HS and HS^3 configurations differ by one localized electron more in the former, which is reflected in the presented DOS (see Figs. 3(a) and 3(b)). The difference is that the first isolated, minority Fe t_{2g} band, lying just below the valence band, is moved above the valence band, coinciding with the Fermi level (see

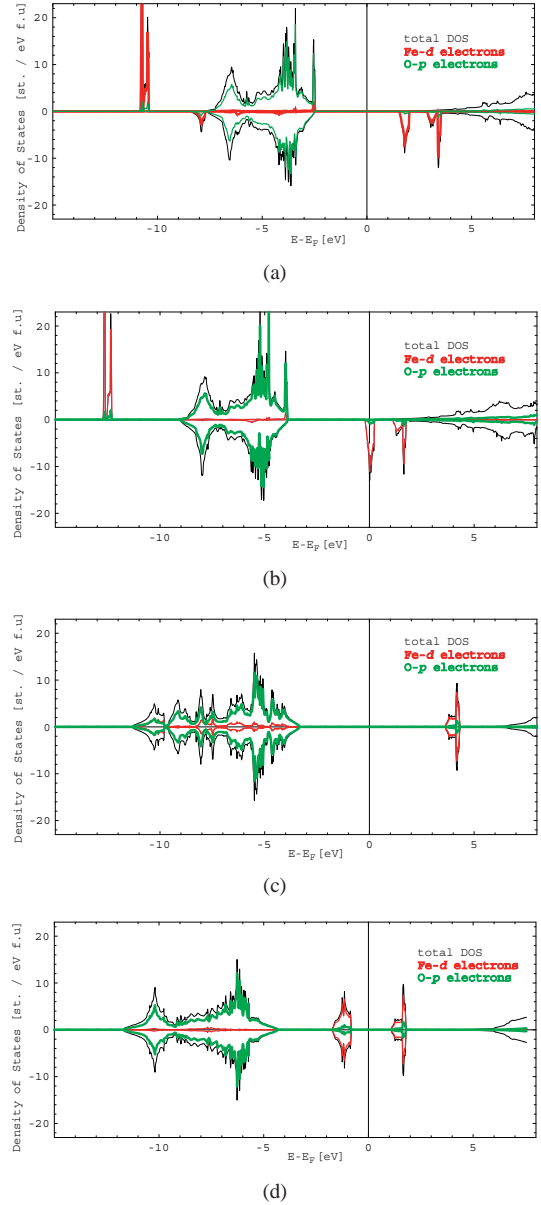


FIG. 3: (a) Spin-resolved density of states (DOS) for HS state as calculated from SIC-LSD at a pressure of 2 GPa and Fe concentration of 12.5%. (b) Spin-resolved density of states for the HS^3 state as calculated from SIC-LSD at a pressure of 2 GPa and Fe concentration of 12.5%. (c) Spin-resolved density of states for the LS state calculated at a pressure of 124 GPa and Fe concentration of 12.5%. (d) Spin-resolved density of states calculated with the standard LSD approximation at 102 GPa and Fe concentration of 12.5%. In all the cases the Fe DOS is in red, while the total DOS is in black and the O 2p DOS in green.

Fig. 3(b)). While for the HS configuration SIC-LSD delivers, in agreement with experiment and other theoretical considerations,^{51,52,53} an insulator of charge transfer character, the HS^3 configuration gives rise to a half-metal, with a large band gap in the majority band, and a metallic behavior in the spin-down channel, with a partially occupied minority Fe d

band at the Fermi level.

At high pressures the LS and LSD configurations are of relevance. The DOS of the LS is shown in Fig. 3(c). It is characterized by hybridized Fe-3*d* electrons with the predominantly O 2*p* valence band, and a large band gap to the Fe *d* conduction band. The lsd DOS shows a substantially reduced band gap, which is between the occupied and unoccupied Fe impurity *d* bands. So, while the SIC-LSD LS state is a charge transfer insulator, the LSD gives rise to a Mott-Hubbard insulator (see Fig. 3(d)).

C. GGA-PAW calculations, Fe clustering

So far we have concentrated mostly on the correlated nature of Fe *d* electrons in describing electronic properties of doped MgO within SIC-LSD approach. Here we consider an importance of a possible Fe impurity clustering. To study this, we have performed a number of independent calculations for low Fe concentrations in $\text{Mg}_{1-x}\text{Fe}_x\text{O}$, using the standard GGA approximation⁵⁴ and the Vienna Ab-Initio Simulation Package (VASP)³⁸. The latter provides the standard projector augmented wave potentials for Mg, Fe and O with core configurations $2p^63s^2$ (Mg), $3p^63d^74s^1$ (Fe) and $2s^22p^4$ (O).⁵⁵ In the actual calculations the electronic optimization has been run with a self-consistency threshold of 10^{-9} eV, ionic optimization has been done with a threshold of 10^{-6} eV. The $4 \times 4 \times 4$ -Monkhorst-Pack scheme has been applied for the k-point sampling, producing four irreducible k-points.⁵⁶ The energy cut-off of the plane wave basis set has been equal to 700 eV. In order to speed up the evaluation of the non-local part of the potentials real space projections have been used. A second order Methfessel-Paxton smearing has been used ($\sigma=0.04$ eV), introducing an error in electronic entropy, $T S_{\text{el}}$, of at most 0.111 meV/atom.⁵⁷ The accuracy of the energy differences between the HS and the LS state has been converged to 1.3×10^{-6} eV/atom. Note, however, that within the GGA implementation all the electrons are treated on equal footing as delocalized, with the HS state being described as a ferromagnetic state, whilst the LS state as a non-magnetic state. Thus the two are not directly comparable to the HS and LS states calculated within SIC-LSD, as the concept of divalent and trivalent ions cannot be clearly defined within GGA.

To investigate the effects of Fe clusters, supercells containing 64 atoms have been set up, including one and four Fe impurities ($x_{\text{Fe}} = 3.125\%$, $x_{\text{Fe}} = 12.5\%$). In the latter case, 30 distinct arrangements of Fe atoms exist.⁷⁰ We have used the most extreme cases, where the Fe atoms form a tetragonal cluster with an Fe-Fe distance of ≈ 2.69 Å and where they avoid each other at a maximal distance of ≈ 5.37 Å (at 100 GPa). The resulting three clusters (one Fe atom, four Fe atoms at minimum distance, four Fe atoms at maximum distance) have been explored performing spin-polarized and non-spin-polarized GGA calculations (in the former case, a starting magnetic moment of $4 \mu_B$ has been assigned to each Fe atom). In the spin-polarized case the Vosko-Wilk-Nusair interpolation for the correlation part of the exchange-correlation functional has been used,⁵⁸. The lowest energy structure has

been found by comparing the enthalpies of all the different structures.

The GGA-PAW calculations in the 64 atomic supercell find HS-LS transition pressures of 26 GPa ($x = 3.125\%$), 30.3 GPa ($x = 12.5\%$, diluted configuration of Fe), and 63.4 GPa ($x = 12.5\%$, clustered configuration of Fe), as calculated from the intersection of the enthalpy curves of the ferromagnetic and non-magnetic results. The lowest enthalpy structures always give a total magnetization of either $\mu = 0.0\mu_B$ (non-magnetic) or $\mu = 4.0\mu_B$ (ferromagnetic). Arrangements of Fe atoms with an intermediate spin magnetic moment have been found in some cases (e.g. $\mu = 3\mu_B$ in the case of Fe clusters between 90 GPa and 185 GPa). However they always turn out to be unstable because energetically lower lying cluster configurations exist.

The transition pressure turns out to increase with the Fe concentration. The two studied concentrations ($x = 3.125\%$ and $x = 12.5\%$) allow to determine the linear dependence of the transition pressure as

$$P_{\text{cr}} = 24.6 + 0.45 x. \quad (11)$$

The relatively small difference to the experimental value of $P_{\text{cr}} = 28 + 0.63 x$ can be explained, if it is assumed that the statistical distribution of the Fe atoms in the experimental sample will not be perfectly diluted, but in some cases result in having Fe atoms at smaller distances (which dramatically raises the critical pressure). However, this can also explain the broadness of the experimentally found transition pressure: depending on the local Fe configuration the spin magnetic moments collapse at different pressures.

Figure 4 indicates that at low pressures (where only the HS arrangements are of interest) the Fe atoms prefer to form clusters, while at high pressures (where only the LS arrangements are of interest) the Fe atoms prefer a diluted configuration. Upon pressure release at the pressure of about 60 GPa the LS diluted arrangement and the HS clustered arrangement coincide. The different Fe arrangements in the high pressure and low pressure regions might hamper this phase transition. Experimental HS-LS transition pressures are predicted to depend on the pressure the sample has been equilibrated at (the equilibration could be enhanced through heat, which accelerates ionic diffusion). If the equilibration is done at high pressure, upon pressure release the LS configuration would be stable up to relatively low pressures (≈ 30 GPa). A sample equilibrated at low pressure on the other hand would preserve its magnetization up to relatively high pressures (≈ 60 GPa).

IV. CONCLUSIONS

Our GGA results indicate a first order transition for all the compositions studied, both for $\text{Mg}_{1-x}\text{Fe}_x\text{O}$ and Fe_{1-x}O , in good agreement with the notion in Ref. 32 for Fe_{1-x}O . The electronic rearrangement of the Fe atoms leads to a discontinuity of the first derivative of the enthalpy, i.e. the volume (see Fig. 4). This affects various physical properties of the HS

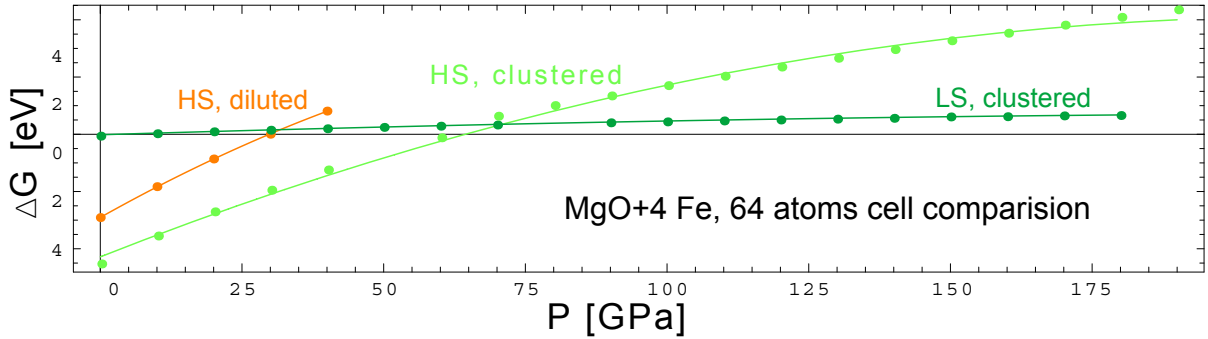


FIG. 4: GGA-PAW calculations, 64 atomic supercell including four Fe atoms: Comparison of the enthalpies of the different Fe and spin arrangements to the diluted LS setting. In the clustered configuration Fe atoms are at the largest distance possible.

and LS phases, such as the zero pressure bulk modulus and the ground state volume.

In experiment the HS-LS transition appears to be smeared out over a large pressure range,^{20,24,36} which in the case of Fe_{1-x}O has led to the conjecture that the transition might be second order.³⁵ We can not support this unless this is a temperature induced smearing which our $T = 0$ calculations do not consider. The results for various Fe arrangements, keeping the Fe concentration fixed, indicate that the local arrangement of Fe strongly influences the spin transition pressure of the Fe atoms. The statistical distribution of the Fe atoms and the short range defect order can therefore smear out the transition pressure over a large pressure range. As the HS-LS transition is isosymmetric, according to Landau theory it can only be first-order or (above the critical temperature) fully continuous.^{59,60}

We can confirm the experimentally found trend that the HS-LS transition pressure increases with increasing Fe concentration. This might be the result of Fe atoms which — if situated closely enough — simultaneously optimize their electronic configurations. These magnetic Fe clusters can not easily be demagnetized by pressure. The increase of the Fe concentration leads to a statistical increase of short Fe-Fe distances, which through the described mechanism could in turn lead to an increase of the critical pressure.

It has been proposed that the HS-LS transition in magnesiowüstite would lead to a discontinuity in the Earth’s lower mantle.²⁰ Although the transition appears to be first order a discontinuity seems to be improbable: first the sensitivity of the transition pressure to the (local) Fe concentration could smear out the transition over a wide region in depth. Second, temperature could further increase this effect and shift the transition to even higher pressures, barring LS Fe^{2+} from the Earth’s interior.^{18,61}

The transition pressures predicted by SIC-LSD appear to be higher which might be a result of an “overcorrection” of the energy of the localized states. It has been argued in Ref. 62 that a weighted self-interaction correction would be desirable. The high transition pressures calculated in this work might

also be due to the fact that the ASA does not allow relaxations of the atomic spheres, which might be significant in the LS phase, where the ionic radius of Fe is small. At high pressures the LSD treatment can lead to low energy structures. This could justify the treatment of $\text{Mg}_{1-x}\text{Fe}_x\text{O}$ at those pressures using standard approximations for the exchange-correlation energy such as the GGA. Apart from this it could also indicate a second phase transition which involves a full delocalization of the Fe-3d states. Furthermore all the transitions considered in this paper involve five or six localized electrons in the high volume phase and no localized electrons in the low volume phase. Consideration of valence fluctuations or ‘intermediate’ localization involving four, three, two and one localized states could plausibly lead to a reduction of the transition pressure. The SIC-LSD formalism, implemented in the multiple scattering theory, allows to consider static valence and spin fluctuations at finite temperatures, by invoking CPA (coherent potential approximation) and DLM (disordered local moments) approaches, which was successfully applied to studying phase diagrams.^{63,64} This would also be useful for the further theoretical investigation of the present geophysically relevant systems. For the nearest future, it may be instructive to first apply SIC-LSD in a full potential version in order to allow for ionic relaxations to study the influence of distortions on the ground state properties of these systems.

Acknowledgements

The authors are indebted to A.R. Oganov who contributed considerably to the concept of this work. DJA thanks A.R. Oganov and the ETH Zurich Research fund for their support of this work (Grant No. TH-27033). Supercomputers were provided by the Swiss National Supercomputing Centre (CSCS) and ETH Zürich. WMT and ZS would like to acknowledge useful discussions with Drs. Axel Svane and Leon Petit.

- * Electronic address: donat.adams@cea.fr
† CEA, DAM, DIF, F 91297 Arpajon, France
- ¹ S. Ono and A. R. Oganov, *Earth Planet. Sci. Lett.* **236**, 914 (2005).
 - ² D. L. Anderson, *Theory of the Earth* (Blackwell Scientific Publications, Oxford, 1989).
 - ³ A. R. Oganov, Ph.D. thesis, University of London (2002).
 - ⁴ A. R. Oganov and P. I. Dorogokupets, *Phys. Rev. B* **67**, 224110 (2003).
 - ⁵ T. S. Duffy, R. J. Hemley, and H. kwang Mao, *Phys. Rev. Lett.* **74**, 1371 (1995).
 - ⁶ J. E. Jaffe, J. A. Snyder, Z. Lin, and A. C. Hess, *Phys. Rev. B* **62**, 1660 (2000).
 - ⁷ H. Zhang and M. S. T. Bukowinski, *Phys. Rev. B* **44**, 2495 (1991).
 - ⁸ K. J. Chang and M. L. Cohen, *Phys. Rev. B* **30**, 4774 (1984).
 - ⁹ B. B. Karki, R. M. Wentzcovitch, S. de Gironcoli, and S. Baroni, *Phys. Rev. B* **61**, 8793 (2000).
 - ¹⁰ N. D. Drummond and G. Ackland, *Phys. Rev. B* **65**, 184104 (2002).
 - ¹¹ G. Kalpana, B. Palanivel, and M. Rajagopalan, *Phys. Rev. B* **52**, 4 (1995).
 - ¹² M. Causà, R. Dovesi, C. Pisani, and C. Roetti, *Phys. Rev. B* **33**, 1308 (1986).
 - ¹³ A. Strachan, T. Çağın, and W. A. Goddard, *Phys. Rev. B* **60**, 15084 (1999).
 - ¹⁴ A. Dewaele, G. Fiquet, D. Andrault, and D. Hausermann, *J. Geophys. Res.* **105**, 2869 (2000).
 - ¹⁵ S. Speziale, C.-S. Zha, T. S. Duffy, R. J. Hemley, and H. Mao, *J. Geophys. Res.* **106**, 515 (2001).
 - ¹⁶ M. Mehl, R. E. Cohen, and H. Krakauer, *J. Geophys. Res.* **93**, 8009 (1988).
 - ¹⁷ K. Persson, A. Bengtson, G. Ceder, and D. Morgan, *Geophys. Res. Lett.* **33** (2006).
 - ¹⁸ T. Tsuchiya, R. M. Wentzcovitch, C. R. S. da Silva, and S. de Gironcoli, *Phys. Rev. Lett.* **96**, 198501 (2006).
 - ¹⁹ Z. Fang, I. V. Solovyev, H. Sawada, and K. Terakura, *Phys. Rev. B* **59**, 762 (1999).
 - ²⁰ J. Badro, G. Fiquet, F. Guyot, J.-P. Rueff, V. V. Struzhkin, G. Vankáo, and G. Monaco, *Science* **300**, 789 (2003).
 - ²¹ A. F. Goncharov, V. V. Struzhkin, and S. D. Jacobsen, *Science* **312**, 1205 (2006).
 - ²² E. Gaffney and D. L. Anderson, *J. Geophys. Res.* **78**, 7005 (1973).
 - ²³ Y. Fei, H. kwang Mao, J. Shu, and J. Hu, *Phys. Chem. Minerals* **18**, 416 (1992).
 - ²⁴ J.-F. Lin, V. V. Struzhkin, S. D. Jacobsen, M. Y. Hu, P. Chow, J. Kung, H. Liu, H. kwang Mao, and R. J. Hemley, *Nature* **436**, 377 (2005).
 - ²⁵ T. Welberry and A. G. Christy, *Phys. Chem. Minerals* **24**, 24 (1997).
 - ²⁶ T. Welberry and A. G. Christy, *J. Solid State Chem.* **117**, 398 (1995).
 - ²⁷ C. Carel and J. Gavarri, *Phys. Chem. Minerals* **26**, 78 (1998).
 - ²⁸ J.-R. Gavarri and C. Carel, *Rev. Chim. Minérale* **18**, 608 (1981).
 - ²⁹ Y. Ding, J. Xu, C. T. Prewitt, R. J. Hemley, H. kwang Mao, and J. A. Cowan, *Applied Phys. Lett.* **86** (2005).
 - ³⁰ Y. Ding, H. Liu, J. Xu, C. T. Prewitt, R. J. Hemley, and H. kwang Mao, *Applied Phys. Lett.* **87**, 041912 (2005).
 - ³¹ Y. Ding, H. Liu, M. Somayazulu, Y. Meng, J. Xu, C. T. Prewitt, R. J. Hemley, and H. kwang Mao, *Phys. Rev. B* **72**, 174109 (2005).
 - ³² S. Ono, Y. Ohishi, and T. Kikegawa, *J. Phys. Cond. Matt.* **19**, 036205 (2007).
 - ³³ S. D. Jacobsen, J.-F. Lin, R. J. Angel, G. Shen, V. B. Prakapenka, D. Przemyslaw, H.-K. Mao, and R. J. Hemley, *J. Synchrotron Radiat.* **12**, 577 (2005), international workshop on Structure Determination by Single-Crystal X-ray Diffraction (SXD) at Megabar Pressures, Chicago, USA (13/11/2004).
 - ³⁴ V. V. Struzhkin, H. kwang Mao, J. Hu, M. Schwoerer-Böhning, J. Shu, R. J. Hemley, W. Sturhahn, M. Y. Hu, E. E. Alp, P. Eng, et al., *Phys. Rev. Lett.* **87**, 255501 (2001).
 - ³⁵ M. P. Pasternak, R. D. Taylor, R. Jeanloz, X. Li, J. H. Nguyen, and C. A. McCammon, *Phys. Rev. Lett.* **79**, 5046 (1997).
 - ³⁶ S. Speziale, A. Milner, V. E. Lee, S. M. Clark, M. P. Pasternak, and R. Jeanloz, *Proc. Natl. Acad. Sci.* **102**, 17918 (2005).
 - ³⁷ J. Badro, V. V. Struzhkin, J. Shu, R. J. Hemley, and H. kwang Mao, *Phys. Rev. Lett.* **83**, 4101 (1999).
 - ³⁸ G. Kresse and J. Furthmüller, *Phys. Rev. B* **54**, 11169 (1996).
 - ³⁹ W. M. Temmerman, A. Svane, Z. Szotek, , and H. Winter, in *Electronic Density Functional Theory: Recent Progress and New Directions*, edited by J. F. Dobson, G. Vignale, and M. P. Das (Plenum, New York, 1998), pp. 327–347.
 - ⁴⁰ O. K. Andersen and O. Jepsen, *Phys. Rev. Lett.* **53**, 2571 (1984).
 - ⁴¹ O. K. Andersen, *Phys. Rev. B* **12**, 3060 (1975).
 - ⁴² W. R. L. Lambrecht and O. K. Andersen, *Phys. Rev. B* **34**, 2439 (1986).
 - ⁴³ R. C. Whited and W. C. Walker, *Phys. Rev. Lett.* **22**, 1428 (1969).
 - ⁴⁴ J.-P. Poirier, *Introduction to the Physics of the Earth's Interior* (Cambridge University Press, Cambridge, UK, 2000).
 - ⁴⁵ F. Birch, *Phys. Rev.* **71**, 809 (1947).
 - ⁴⁶ Z. Szotek, W. M. Temmerman, A. Svane, L. Petit, G. M. Stocks, and H. Winter, *Phys. Rev. B* **68**, 054415 (2003).
 - ⁴⁷ D. Kasinathan, J. Kuneš, K. Koepfner, C. V. Diaconu, R. L. Martin, I. D. Prodan, G. E. Scuseria, N. Spaldin, L. Petit, T. C. Schulthess, et al., *Phys. Rev. B* **74**, 195110 (2006).
 - ⁴⁸ M. Däne, M. Lüders, A. Ernst, D. Ködderitzsch, W. M. Temmerman, Z. Szotek, and W. Hergert, *Journal of Physics: Condensed Matter* **21**, 045604 (2009).
 - ⁴⁹ A. Svane, P. Strange, W. M. Temmerman, and Z. Szotek, *Phys. Stat. Sol.* **223**, 105 (2001).
 - ⁵⁰ T. Tsuchiya, R. M. Wentzcovitch, C. R. S. da Silva, S. de Gironcoli, and J. Tsuchiya, *Phys. Stat. Sol. B* **243**, 2111 (2006).
 - ⁵¹ F. Parmigiani and L. Sangaletti, *Journal of Electron Spectroscopy and Related Phenomena* **98-99**, 287 (1999).
 - ⁵² G. A. Sawatzky and J. W. Allen, *Phys. Rev. Lett.* **53**, 2339 (1984).
 - ⁵³ J. Zaanen, G. A. Sawatzky, and J. W. Allen, *Phys. Rev. Lett.* **55**, 418 (1985).
 - ⁵⁴ J. P. Perdew, K. Burke, and M. Ernzerhof, *Phys. Rev. Lett.* **77**, 3865 (1996).
 - ⁵⁵ G. Kresse and D. Joubert, *Phys. Rev. B* **59**, 1758 (1999).
 - ⁵⁶ H. J. Monkhorst and J. D. Pack, *Phys. Rev. B* **13**, 5188 (1976).
 - ⁵⁷ M. Methfessel and A. T. Paxton, *Phys. Rev. B* **40**, 3616 (1989).
 - ⁵⁸ S. Vosko, L. Wilk, , and M. Nusair, *Can. J. Phys.* **58**, 1200 (1980).
 - ⁵⁹ A. G. Christy, *Acta Cryst.* **B51**, 753 (1995).
 - ⁶⁰ A. D. Bruce and R. Cowley, *Structural phase transitions* (Taylor & Francis, London, 1981).
 - ⁶¹ W. Sturhahn, J. M. Jackson, and J.-F. Lin, *Geophys. Res. Lett.* **32** (2005).
 - ⁶² J. P. Perdew, A. Ruzsinszky, J. Tao, V. N. Staroverov, G. E. Scuseria, and G. I. Csonka, *J. Chem. Phys.* **123**, 062201 (2005).
 - ⁶³ M. Lüders, A. Ernst, M. Däne, Z. Szotek, A. Svane, D. Ködderitzsch, W. Hergert, B. L. Gyorffy, and W. M. Temmerman, *Phys. Rev. B* **71**, 205109 (2005).
 - ⁶⁴ I. D. Hughes, M. Däne, A. Ernst, W. Hergert, M. Lüders, J. Poulter, J. B. Staunton, A. Svane, Z. Szotek, and W. M. Temmerman,

Nature **446**, 650 (2007).

- ⁶⁵ The nominal valence $N_{\text{val}} = Z - N_{\text{core}} - N_{\text{SIC}}$ does not always correspond to the chemical valence. For example, in the case of the conventional LSD scheme the valence of Fe would be $N_{\text{val}} = Z - N_{\text{core}} - N_{\text{SIC}} = 26 - 18 - 0 = 8$.
- ⁶⁶ We have used a standard procedure such as provided with the EXCITING code at <http://exciting.sourceforge.net>.
- ⁶⁷ The enthalpy differences have been fitted to the second order polynomials. However, the error resulting from these fits and the numerical inversion of Eq. 8 have given rise to total errors of the order $10^{-8} - 10^{-12}$ eV/atom.
- ⁶⁸ ΔE is given for one supercell containing 2 Mg, 2 Fe and 4 O in the first case and 4 Fe and 4 O in the second.
- ⁶⁹ In our calculations the Fe-ASA radii were fixed to those of Mg at ambient conditions. According to Anderson² they are comparable: $r_{\text{Mg}} = 0.72 \text{ \AA}$, $r_{\text{Fe,HS}} = 0.77 \text{ \AA}$. However, in the LS phase the radius of Fe dramatically reduces to 0.61 \AA . Due to the LMTO-ASA approach, the reduction of the ionic radii could not be taken into account.
- ⁷⁰ Note that this is a combinatorial problem. The clusters can be characterized by the distance between the first Fe impurity to the following ones. Five different distances can be found in the 64 atomic cell. They can host 12, three, 12, three and one Fe atom respectively. This gives one, five, 14, 30, 53 distinct scenarios of one, two, three, four and five impurities, respectively.